metals

MDPI

Article

Effect of Rolling Temperature on the Structural Refinement and Mechanical Properties of Dual-Phase Heterostructured Low-Carbon Steel

Tao Xu [1,†], Zhiyi Pan [1,†], Bo Gao [1,*], Jiaxi Huang [1], Xuefei Chen [2,3], Yi Liu [1], Lirong Xiao [1,*] and Hao Zhou [1]

[1] Nano and Heterogeneous Materials Center, School of Materials Science and Engineering, Nanjing University of Science and Technology, Nanjing 210094, China; xt971107@njust.edu.cn (T.X.); zhiyipan0602@163.com (Z.P.); huangjiaxi@njust.edu.cn (J.H.); liuyi9280@njust.edu.cn (Y.L.); hzhou511@njust.edu.cn (H.Z.)
[2] State Key Laboratory of Nonlinear Mechanics, Institute of Mechanics, Chinese Academy of Sciences, Beijing 100190, China; chenxuefei@lnm.imech.ac.cn
[3] School of Engineering Science, University of Chinese Academy of Sciences, Beijing 100049, China
* Correspondence: gaobo@njust.edu.cn (B.G.); xiaolr620@njust.edu.cn (L.X.)
† These authors contributed equally to this work.

Abstract: Warm rolling at temperatures ranging from 25 °C to 500 °C was conducted on the dual-phase heterostructured low-carbon steel to investigate the effect of deformation temperature on the structural refinement and mechanical properties. Defying our intuition, the grain size and strength of the rolled steels do not deteriorate with the increase in deformation temperature. Warm rolling at 300 °C produces a much finer lamellar structure and higher strength than steels rolled at both room temperature and elevated temperature. It is supposed that the enhanced interactions between carbon atoms and defects (interfaces and dislocations) at 300 °C promote dislocation accumulation and stabilize the nanostructure, thus helping with producing an extremely finer structure and higher strength than other temperatures.

Keywords: heterostructure; dual-phase steel; warm rolling; interstitial atoms; high strength

Citation: Xu, T.; Pan, Z.; Gao, B.; Huang, J.; Chen, X.; Liu, Y.; Xiao, L.; Zhou, H. Effect of Rolling Temperature on the Structural Refinement and Mechanical Properties of Dual-Phase Heterostructured Low-Carbon Steel. *Metals* **2022**, *12*, 115. https://doi.org/10.3390/met12010115

Academic Editor: Soran Birosca

Received: 5 December 2021
Accepted: 6 January 2022
Published: 7 January 2022

1. Introduction

High-strength steels with low cost are highly desired in advanced industries for weight reduction and environmental conservation [1–3]. Numerous approaches have been developed to produce high-strength steels, among which increasing the additional alloy contents is the most efficient. Maraging steels containing many expensive elements, e.g., Ni, Co, Mo, Ti, usually have ultra-high strength above 2 GPa [4,5]. However, the strategy of alloying has a negative impact on the long-term sustainability of high-performing metals [6,7]. Therefore, alternative approaches to strengthening steel need to be explored.

In recent decades, severe plastic deformation (SPD) techniques have been widely developed to produce ultra-strong nanostructured materials [8,9]. The grain size of metallic materials can be refined to ultra-fine grain (1000 to 100 nm) or even nanocrystalline (<100 nm) by applying a large equivalent strain ($\varepsilon > 4$) [10,11]. The grain size of the low-carbon martensitic steel was refined to 100 nm by high-pressure torsion (HPT), which has an ultra-high strength of 2.4 GPa [12]. However, the major issues for using SPD techniques to produce ultra-high-strength materials include scaling-up and cost in industrial-scale productions.

Industrial rolling is a widely used method to produce bulk metallic plates with high efficiency and economy. Nevertheless, the lower equivalent strain compared to SPD techniques limits the efficiency of grain refinement [13–18]. To extremely refine the microstructure through conventional rolling, the initial structure and processing route should be carefully tailored. Deformation-induced structural refinement is governed by the competition among dislocation generation, dynamic recovery, recrystallization, and grain boundary

migration [19–22]. Structural refinement is enhanced if dislocation generation is enhanced or if dynamic recovery and recrystallization are suppressed during the deformation process [23,24]. Considering these factors, a novel processing route of heterostructure and interstitial mediated warm rolling was proposed in the previous study [25], which produces an ultra-strong low-carbon nano-steel with a record-breaking average lamellar thickness of 17.8 nm. Warm rolling of dual-phase heterostructured steel improves the deformation compatibility of constituent phases and boosts dislocation multiplication [25]. In addition, at the elevated temperature of 300 °C, the encouraged segregation of interstitial atoms at interfaces helps with stabilizing the nano-structure [26–28]. Therefore, this strategy of warm rolling on the dual-phase heterostructure can produce bulk nano-steel with ultra-high strength of 2.15 GPa under a much lower equivalent strain than conventional SPD techniques. However, the effects of rolling temperatures on the microstructure and mechanical properties of the dual-phase heterostructured low-carbon steels have not been systematically explored.

In the present study, warm rolling at temperatures ranging from 25 °C to 500 °C was carried out on the dual-phase heterostructured low-carbon steel. The microstructure and mechanical properties of the high-strength steels are systematically explored. The effects of deformation temperature on the structural refinement of the dual-phase heterostructured steel are discussed in detail.

2. Materials and Methods

2.1. Processing Route

The chemical composition of the studied low-carbon steel is Fe-0.19C-1.46Si-1.01Mn in weight percent, which is determined by a vacuum emission spectroscopy (ThermoFisher, Waltham, MA, USA). The processing route to develop ultra-strong steels is divided into three steps, which was recommended in the previous study [25]. First, the samples were austenitized at 950 °C for 60 min followed by water quenching to obtain a martensitic microstructure. Then, an intercritical annealing at 820 °C for 10 min was performed to produce a dual-phase heterostructure containing ferrite and martensite. Finally, the dual-phase steel sheets were warm rolled at different temperatures (25, 150, 250, 300, 400, and 500 °C). Before rolling, the steel samples with a thickness of 8 mm and width of 30 mm were preheated at the designated temperatures for 20 min. The thickness reduction of each pass was ~0.5 mm, and the samples were reheated in the furnace (Kejing Material Technology Co., LTD., Hefei, China) for 5 min after each pass. The sheets were rolled from 8 mm to 1.2 mm, with a total thickness reduction of 85%.

2.2. Microstructural Characterization

The cross-section samples were ground, polished and etched with 2% Nital solution. The microstructures were observed by scanning electron microscopy (SEM, FEI Quanta 250F, FEI, Hillsboro, OR, USA). According to the SEM images, the volume fraction of martensite of the dual-phase steel was quantitatively analyzed by using Image J software (V1.46r) [29]. The substructures of DP steels were also characterized by a transmission electron microscope (TEM, FEI Tecnai 20, FEI, Hillsboro, OR, USA) operated at 200 kV. The TEM foils were cut parallel to the transverse plane and ground to a thickness of ~20 μm. Finally, the foils were thinned by ion milling at −30 °C.

2.3. Tests of Mechanical Properties

Dog bone-shaped tensile specimens with a gauge length of 10 mm and width of 2.5 mm were cut from the steel plates with the longitudinal axes parallel to the rolling direction. The tensile specimens were polished to a mirror finish before tensile tests. Quasi-static uniaxial tensile tests were performed on an LTM-20KN testing machine (Walter + Bai, Löhningen, Switzerland) with a strain rate of 3×10^{-3} s^{-1} at room temperature. Vickers hardness was measured by an HMV-G hardness tester (Shimadzu, Tokyo, Japan) with a load of 500 g and

a holding time of 15 s. The microhardness values were obtained by averaging at least ten indentations in each sample.

3. Results

3.1. Microstructure Prior to Warm Rolling

Figure 1a shows the microstructure of the low-carbon steel quenched at 950 °C. A typical lath martensitic structure is obtained. The prior austenite grain boundaries (PAGBs) are marked by the yellow dash lines, indicating that the average grain size is ~30 μm. The austenite grain is divided into a hierarchical structure containing packets, blocks and laths with certain orientation relationships, which are reported in [30–33]. The average lamellar thickness of the lath martensite is ~0.74 μm. As shown in Figure 1b, when the martensitic steel was annealed at 820 °C for 10 min, a typical dual-phase heterostructure containing 47 vol% ferrites and 53 vol% martensites is formed, exhibiting a fibrous morphology which inherits from the lath martensite structure [34]. The average lamellar thicknesses of the fibrous ferrite and martensite are 1.3 μm and 0.6 μm, respectively. Therefore, the dual-phase heterostructured steel with a fine structure for subsequent rolling is obtained through the prior two steps of the processing route.

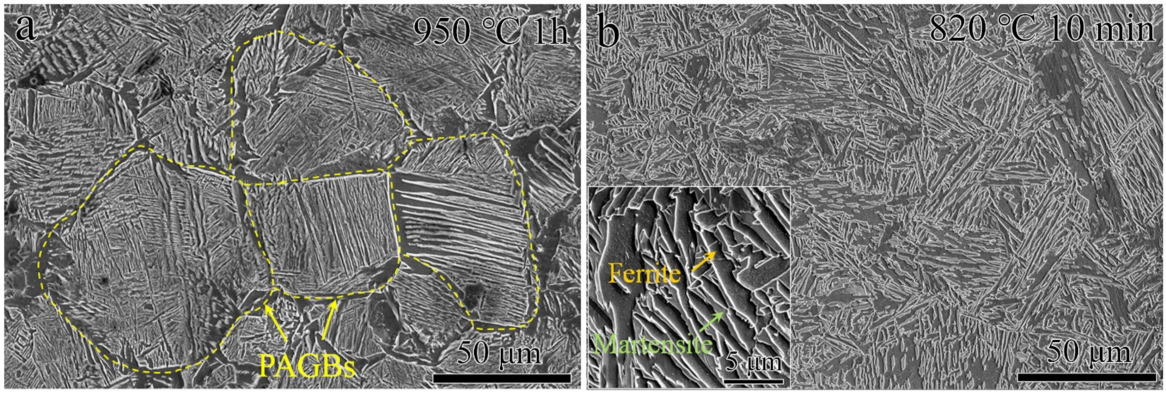

Figure 1. SEM micrographs of (**a**) lath martensite structure after austenitizing at 950 °C for 60 min and water quenching, (**b**) fibrous DP microstructures after subsequent intercritical austenitizing at 820 °C for 10 min and water quenching.

3.2. Microstructures after Warm Rolling

Figure 2 shows the SEM micrographs of the dual-phase steels rolled at different temperatures with a thickness reduction of 85%. Figure 2a shows the SEM morphology of the sample rolled at room temperature (25 °C, cold rolling). Cold rolling leads to the alignment of phase zones parallel to the rolling direction. However, with an 85% thickness reduction, some martensitic regions in the cold-rolled sample are still more than 3 μm in thickness. The refinement of the martensitic phase is not sufficient because the strong martensitic phase only carries a small fraction of global plastic strain, which is induced by the significant stain partitioning [35,36]. As shown in Figure 2b, the sample rolled at 150 °C presents a similar morphology with large blocky martensite as the cold-rolled sample. As the rolling temperature increases to 250 °C (Figure 2c), although most of the martensite still exists with a large thickness, some intersecting co-shear bands with angles of ~55° are formed. In the region of shear bands, both ferrite and martensite can be refined effectively. Warm rolling at 300 °C leads to the substantial refinement of both ferrite and martensite phases and produces a higher density of co-shear bands, as pointed in Figure 2d. A higher rolling temperature of 400 °C (Figure 2e) results in a stretched microstructure along the rolling direction and a decrease in the shear band's density. As the rolling temperature is further increased to 500 °C, the shear bands disappear and the lamellar microstructure aligned along the rolling direction is generated. In addition, it is revealed from the inset of Figure 2f that the martensite was resolved at 500 °C, resulting

in the carbides mainly distributed at the lamellae boundaries. The above SEM images show that the stability of martensite decreases with the increase in rolling temperature, leading to changes in the volume fraction of martensite at high temperatures. From 25 °C to 250 °C, the volume fraction of martensite is almost unchanged, indicating a relatively stable condition of the martensitic phase. As the rolling is performed at 300 °C, the microstructure is refined significantly, and the two phases can hardly be distinguished from SEM morphologies. When the rolling temperature is increased to 400 °C, the stability of martensite deteriorates rapidly. A large number of carbides form in the decomposed martensite, resulting in a decrease in the martensite volume fraction. The decreased stability of martensite is related to the increased carbide precipitation kinetics with an increase in rolling temperatures [37,38]. As reported in [38], the progress of martensite tempering and carbide precipitation can be distinguished into three stages from 120 °C to 500 °C. The first stage is from 120 °C to 195 °C, accompanied by the formation of the transitional carbides (Fe_2C and/or $Fe_{2.4}C$). The second one involves the formation of Hägg-carbide at temperatures of 220–350 °C. The third tempering stage is above 300 °C, in which the decomposition of martensite into a mixture of ferrite and cementite (Fe_3C).

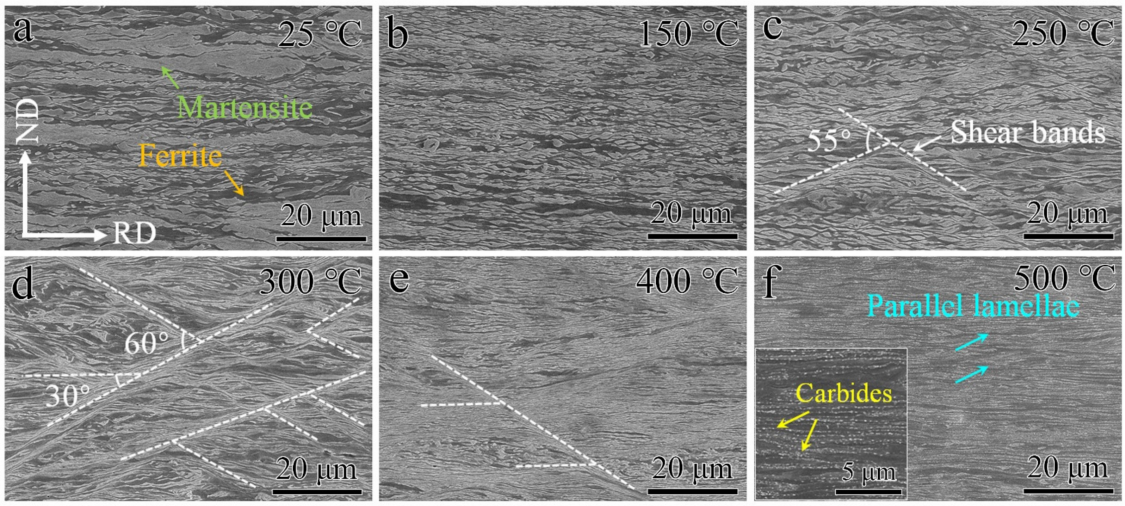

Figure 2. SEM morphologies of the dual-phase heterostructured steel rolled at different temperatures with 85% thickness reduction: (**a**) 25 °C, (**b**) 150 °C, (**c**) 250 °C, (**d**) 300 °C, (**e**) 400 °C, (**f**) 500 °C.

It is found that the deformation temperature has a great influence on the microstructural evolution during rolling. TEM observations on typical samples rolled at 25, 300 and 500 °C were carried out to investigate the effect of rolling temperature on the structural refinement of dual-phase steels. It can be seen from the bright-field TEM micrographs of Figure 3a–c that rolling deformation produces a lamellar structure parallel to the rolling direction. No obvious carbides are observed in the samples rolled at room temperature and 300 °C. However, when rolling at 500 °C, a large number of carbides ~100 nm in size appear preferentially at the lamellar interfaces, as shown in Figure 3c. As indicated in Figure 3d–f, the rolling temperature has strong effects on the microstructural refinement. At the same rolling reduction of 85%, warm rolling at 300 °C produces an average lamellar thickness of 22 nm, which is much thinner than that produced by cold rolling (58 nm). This is coincident with our previous study [25]. As the rolling temperature further increases to 500 °C, the average lamellar thickness coarsens to 110 nm. As a result, in terms of the low-carbon dual-phase steel in the present study, warm rolling at the intermediate temperature of 300 °C presents superior efficiency in structural refinement than other deformation temperatures at the same equivalent strain of ~1.9.

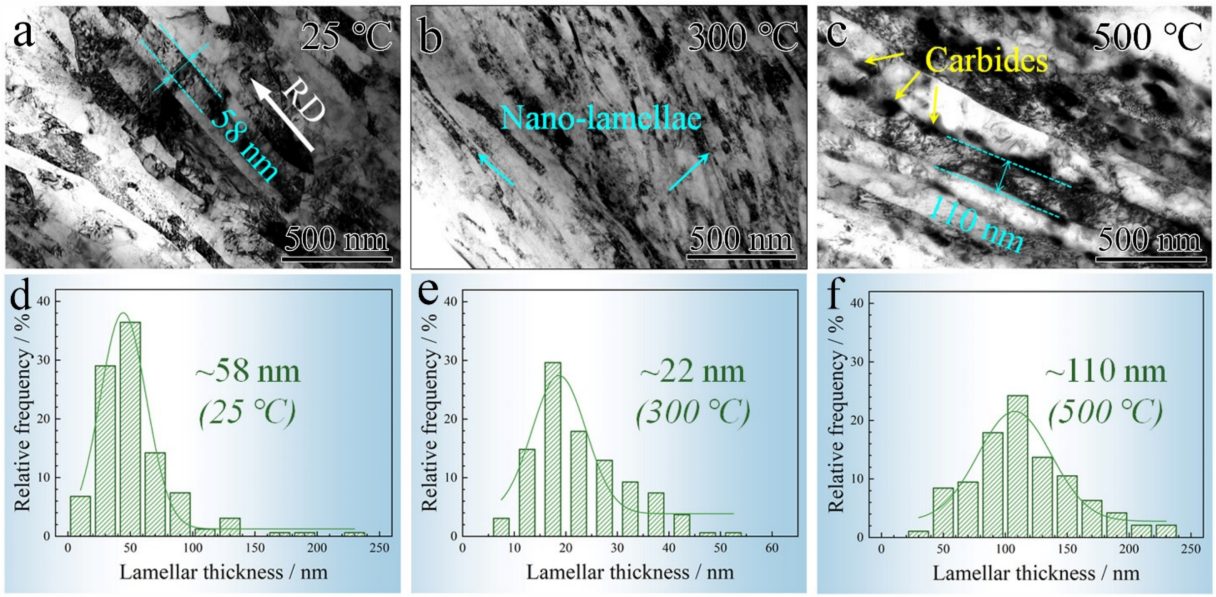

Figure 3. Bright-field TEM micrographs of the dual-phase steels rolled at (**a**) 25 °C, (**b**) 300 °C, (**c**) 500 °C, (**d**–**f**) distribution of lamellar thickness for samples rolled at 25 °C, 300 °C, and 500 °C, respectively.

3.3. Microhardness Evolution of the Rolled Samples

Figure 4a shows the microhardness evolution of the rolled samples with deformation temperatures. For comparison, the microhardness of undeformed dual-phase steel annealed at different temperatures (150, 250, 300, 400, and 500 °C) for 1.5 h is also presented. The annealing time of 1.5 h is close to the total annealing time for the completion of warm rolling. As the deformation temperature increases from 25 °C to 150 °C and 200 °C, the microhardness of the rolled sample slightly increases from 477 HV to 486 HV and 506 HV. The microhardness of the sample warm rolled at 300 °C then sharply increases up to 601 HV. With further increasing rolling temperature to 400 and 500 °C, the microhardness of the rolled samples declines gradually to 510 HV and 388 HV, respectively. In contrast, the microhardness of the undeformed sample keeps ~280 HV when annealed from 25 °C to 300 °C, and slightly decreased at 400 °C. Figure 4b shows the microhardness variation of the warm-rolled sample (300 °C) annealed at different temperatures (300 °C, 400 °C, 500 °C, and 600 °C). It is found that the microhardness is nearly unchanged after annealing at 300 °C for 4 h. When annealed at 400 °C for 1 h, the microhardness of the warm-rolled sample is decreased to 536 HV, and then reaches a plateau. Further increases in the annealing temperature to 500 °C and 600 °C lead to a rapid decrease in the microhardness to 384 HV and 203 HV, respectively. As a result, the nano-lamellar sample warm rolled at 300 °C shows remarkable thermal stability at 300 °C, which is consistent with the results from the in situ TEM observation annealed at 300 °C in the previous study [25].

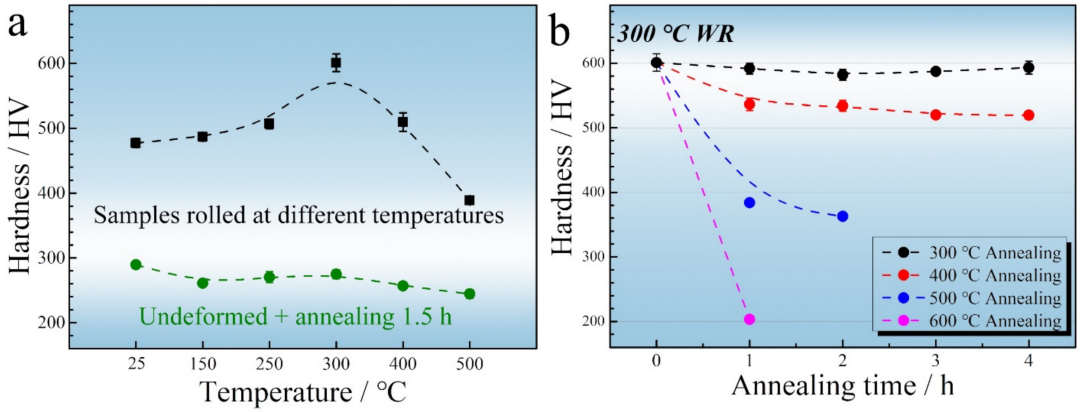

Figure 4. Evolution of the microhardness: (**a**) microhardness of the samples rolled at different temperatures with 85% thickness reduction and the undeformed samples annealed at different temperatures for 1.5 h, (**b**) microhardness of the warm-rolled sample (300 °C) annealed at different temperatures.

3.4. Mechanical Properties

The engineering stress–strain curves of samples rolled at different temperatures are presented in Figure 5a. In addition, the evolution of the yield strength (YS), ultimate tensile strength (UTS) and total elongation (TE) with rolling temperature is shown in Figure 5b. All the samples show continuous yielding behavior, and the stress at a strain of 0.2% is taken as YS. Similar to the results of microstructural refinement, the strength of the rolled samples shows nonmonotonic variation with deformation temperatures. The YS and UTS first increase and then decrease with the rolling temperature, reaching the maximum at 300 °C. The nano-lamellar steel rolled at 300 °C has an extremely high YS of 1.95 GPa and UTS of 2.1 GPa, which is 30% higher than cold rolling (YS: 1.55 GPa, UTS: 1.64 GPa). In comparison, the elongation exhibits an opposite trend with deformation temperatures, arriving at the minimum at 300 °C.

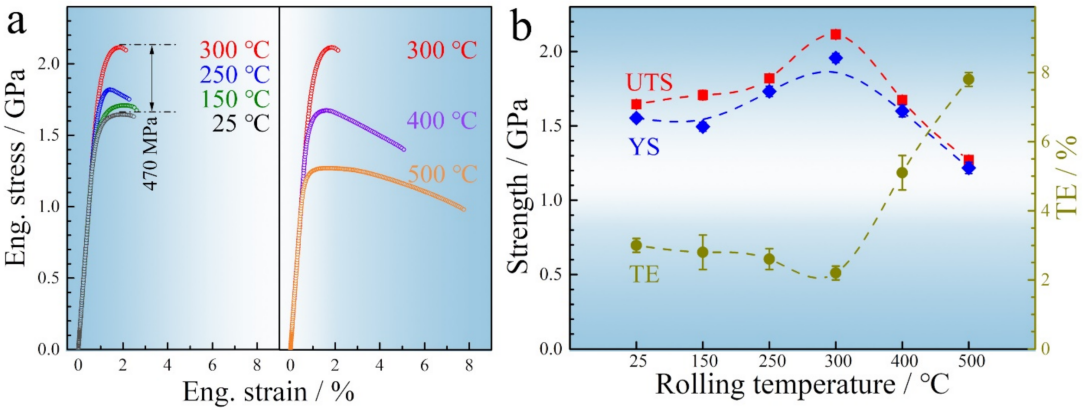

Figure 5. Tensile properties of the rolled samples: (**a**) engineering stress–strain curves, (**b**) evolution of YS, UTS and TE with rolling temperatures.

4. Discussion

4.1. Structural Refinement by Warm Rolling

Defying our intuition, the structural refinement does not deteriorate with the increase in deformation temperature. Warm rolling at 300 °C produces a much finer lamellae structure than that formed at both low temperatures and elevated temperatures. According to the SEM morphologies in Figure 2 and the results in the previous study [23], it is supposed that the key factor influencing the structural refinement during warm rolling is

the responses of martensite, especially the interstitial atoms (carbon, C) in martensite, at different rolling temperatures.

During intercritical annealing, carbon diffuses into the austenitic phase and thus is concentrated in the martensite after quenching [39], as illustrated in Figure 6a. The concentrated carbon and high density of dislocations make martensite much stronger than ferrite. Due to the huge difference in strength between ferrite and martensite, significant strain and stress partitioning occur during cold rolling at 25 °C [40,41], leading to the ferritic lamellae sustaining most of the plastic strain. However, the stress transferred to martensite is not enough to effectively deform them. At the same time, local stress concentrations will break the martensitic lamellae instead of uniformly deforming them.

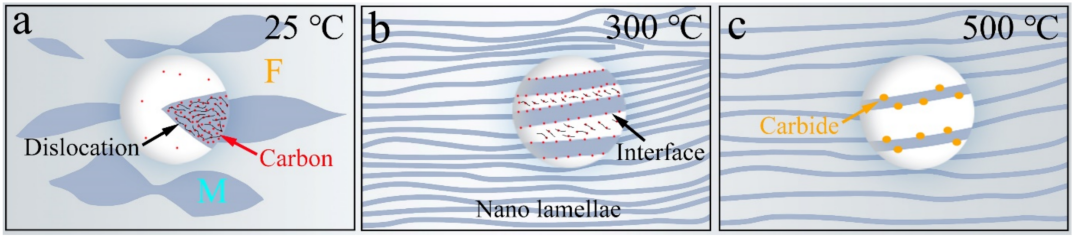

Figure 6. Schematic illustration of the responses of carbon atoms in martensite at different rolling temperatures: (**a**) 25 °C, (**b**) 300 °C, (**c**) 500 °C.

Increasing the rolling temperature to 300 °C, the decreased strength of martensite enables sustained plastic strain larger than cold rolling, as indicated by the high density of co-shear bands in Figure 2d. More importantly, the motion of C atoms is promoted at 300 °C. On the one hand, previous studies [25,42,43] reported that the supersaturated carbon in martensite and the high density of defects induced by rolling promote C atoms segregation at the lamellar boundaries and diffusion into ferrite at elevated temperatures. The segregation of C atoms at grain boundaries enhances the stability of the nano-structure. On the other hand, the interaction between carbon atoms and dislocations during warm deformation is significantly enhanced, which is similar to the phenomenon of dynamic strain aging (DSA) during tensile deformation [44–47]. In regard to DSA, C and N atoms diffuse to dislocation cores at a temperature from 150 °C to 300 °C, which forms so-called Cottrell clouds. The Cottrell clouds exert a pinning effect on dislocations and inhibit dislocation movement. For further plastic deformation, more mobile dislocations must be generated, which enhances the strain hardening rate. In previous studies, Ekrami [48] and Queiroz [49] performed tensile tests on the DP steel samples at temperatures from 25 °C to 600 °C. They found that the tensile strength of DP steels increased with increasing temperature and then decreased at higher temperatures. It is believed that the increase in tensile strength results from the locking of dislocations by carbon atoms in DSA. In the present study, grain refinement and tensile strength of the warm rolled samples are also increased with increasing temperature to 300 °C and then decreased at higher temperatures, which implies strong interactions between C atoms and defects (lamellar boundaries and dislocations) at 300 °C. Additionally, the dense shear bands that occurred in the sample rolled at 300 °C (Figure 2d) also indicate the strong resistance to dislocation glide because the shear band is an alternative deformation mechanism when dislocation activities are impeded [50]. Therefore, the grain refinement mechanism at 300 °C is shown in Figure 6b. At the higher temperature, C atoms with enhanced mobility tend to be segregated at lamellar boundaries and dislocation cores. This redistribution of C atoms can be completed within a period of time. Thus, the inter-pass annealing for 5 min decreases the strength of martensite and provides enough time for the completion of carbon redistribution. Carbon segregation at lamellar boundaries and dislocation cores helps with maintaining the stability of nano-structure and promoting dislocation accumulation, thus producing a significantly refined nano-lamellar structure with an average spacing of 22 nm.

A further increase in rolling temperature to 500 °C results in the precipitation of carbon by forming a large number of carbides, as shown in the schematic of Figure 6c. In this case, the strength of tempered martensite decreases rapidly due to the reduction in carbon content and dislocation density [51], which enables martensite to be co-deformed with ferrite, thus producing a lamellar structure parallel to the rolling direction. However, the higher deformation temperature also accelerates dynamic recovery and recrystallization [52,53], resulting in the coarsening of lamellar thickness.

4.2. Strengthening of the Nano-Lamellar Steels

Previous studies [54–56] have reported that nano-lamellar metals show ultra-high hardness and strength. It is found that the strength acts as a function of the average lamellar thickness (d), and is usually induced by three mechanisms: (i) the pile-up of dislocations at the interfaces from submicron to micron range; (ii) the confined layer slip mechanism from few to few tens of nanometers; (iii) the interface crossing mechanism for about 1–2 nm. As d is larger than 5 nm, the strength of the nano-lamellar metals increases with decreasing lamellar thickness, which is controlled by the (i) and (ii) mechanisms. Figure 7 shows the relationship between the d and YS of the nano-lamellar steels in the present study and [23]. It is clear that the YS of the nano-lamellar steels increases linearly with $d^{-1/2}$, which is consistent with the Hall–Petch relationship. Therefore, the refined lamellar thickness of 22 nm provides a large number of interfaces against dislocation motion [55], which makes the dominant contribution to the ultra-strong strength of 2.1 GPa.

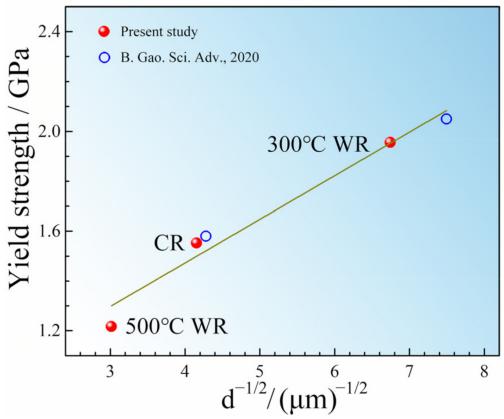

Figure 7. Relationship between YS and lamellar thickness in the nano-lamellar steels. Data from [25].

5. Conclusions

In the present study, rolling with a total thickness reduction of 85% was conducted on the dual-phase heterostructured low-carbon steel at temperatures from 25 °C to 500 °C. Effects of rolling temperature on the microstructural refinement and mechanical properties of the dual-phase heterostructured low-carbon steel are explored. The key conclusions are as follows:

1. The rolling temperature has a great influence on the microstructural refinement of low-carbon dual-phase steel. The average lamellar thickness does not deteriorate with increasing deformation temperature. Warm rolling at 300 °C produces a much finer nano-lamellar structure (22 nm) than that formed at both room temperature and elevated temperatures.
2. The microhardness and strength first increase and then decrease with rolling temperature, reaching the maximum at 300 °C. The nano-lamellar steel has an extremely high hardness of 601 HV and UTS of 2.1 GPa. The microhardness of the nano-lamellar steel also remains stable when annealed at 300 °C.
3. The structural refinement of the heterostructured low-carbon steel is mainly influenced by the responses of C atoms in martensite at different rolling temperatures. At 25 °C,

the supersaturated C in martensite leads to a huge difference in strength between martensite and ferrite. Therefore, the martensite cannot be deformed sufficiently. At an elevated temperature of 300 °C, the motion of C atoms is promoted, which tends to be segregated at lamellar boundaries and mobile to dislocations. These interactions between C atoms and defects promote dislocation accumulation and improve the stability of nano-structure, helping with grain refinement. At a higher temperature of 500 °C, carbides formation in the tempered martensite and enhanced dynamic recovery results in an increase in the average lamellar thickness.

Author Contributions: Conceptualization, H.Z.; methodology, T.X., Z.P.; investigation, J.H., X.C. and Y.L.; writing—original draft preparation, T.X.; writing—review and editing, B.G., L.X. and H.Z.; visualization, T.X.; supervision, H.Z.; funding acquisition, B.G., L.X. and H.Z. All authors have read and agreed to the published version of the manuscript.

Funding: This work was supported by the National Key R&D Program of China (grant number 2021YFA1200203), the Key Program of National Natural Science Foundation of China (grant number 51931003), the National Natural Science Foundation of China (grant numbers 52071178, 51901103), the Hong Kong Research Grants Council (GRF 11214121), the Projects in Science and Technique Plans of Ningbo City (grant number 2019B10083), the China Post-doctoral Science Foundation (grant number 2021M701715) and the Natural Science Foundation of Jiangsu Province (grant number BK20211197).

Acknowledgments: For the technical support we thank the Jiangsu Key Laboratory of Advanced Micro & Nano Materials and Technology. The SEM and TEM experiments are performed at the Materials Characterization and Research Center of Nanjing University of Science and Technology.

Conflicts of Interest: The authors declare no conflict of interest.

References

1. Liu, L.; Yu, Q.; Wang, Z.; Ell, J.; Huang, M.X.; Ritchie, R.O. Making ultrastrong steel tough by grain-boundary delamination. *Science* **2020**, *368*, 1347–1352. [CrossRef] [PubMed]
2. Tan, C.; Chew, Y.; Duan, R.; Weng, F.; Sui, S.; Ng, F.L.; Du, Z.; Bi, G. Additive manufacturing of multi-scale heterostructured high-strength steels. *Mater. Res. Lett.* **2021**, *9*, 291–299. [CrossRef]
3. Lesch, C.; Kwiaton, N.; Klose, F.B. Advanced High Strength Steels (AHSS) for Automotive Applications—Tailored Properties by Smart Microstructural Adjustments. *Steel Res. Inter.* **2017**, *88*, 1700210. [CrossRef]
4. Jiang, S.H.; Xu, X.Q.; Li, W.; Peng, B.; Wu, Y.; Liu, X.J.; Wang, H.; Wang, X.Z.; Lu, Z.P. Strain hardening mediated by coherent nanoprecipitates in ultrahigh-strength steels. *Acta Mater.* **2021**, *213*, 116984. [CrossRef]
5. Jiang, S.; Wang, H.; Wu, Y.; Liu, X.; Chen, H.; Yao, M.; Gault, B.; Ponge, D.; Raabe, D.; Hirata, A.; et al. Ultrastrong steel via minimal lattice misfit and high-density nanoprecipitation. *Nature* **2017**, *544*, 460–464. [CrossRef]
6. Li, X.; Lu, K. Playing with defects in metals. *Nat. Mater.* **2017**, *16*, 700–701. [CrossRef]
7. Li, X.; Lu, K. Improving sustainability with simpler alloys. *Science* **2019**, *364*, 733–734. [CrossRef]
8. Valiev, R.Z.; Estrin, Y.; Horita, Z.; Langdon, T.G.; Zehetbauer, M.J.; Zhu, Y.T. Fundamentals of Superior Properties in Bulk NanoSPD Materials. *Mater. Res. Lett.* **2016**, *4*, 1–21. [CrossRef]
9. Estrin, Y.; Vinogradov, A. Extreme grain refinement by severe plastic deformation: A wealth of challenging science. *Acta Mater.* **2013**, *61*, 782–817. [CrossRef]
10. Cao, Y.; Ni, S.; Liao, X.; Song, M.; Zhu, Y. Structural evolutions of metallic materials processed by severe plastic deformation. *Mater. Sci. Eng. R* **2018**, *133*, 1–59. [CrossRef]
11. Estrin, Y.; Beygelzimer, Y.; Kulagin, R.; Gumbsch, P.; Fratzl, P.; Zhu, Y.; Hahn, H. Architecturing materials at mesoscale: Some current trends. *Mater. Res. Lett.* **2021**, *9*, 399–421. [CrossRef]
12. Müller, T.; Kapp, M.W.; Bachmaier, A.; Felfer, P.; Pippan, R. Ultrahigh-strength low carbon steel obtained from the martensitic state via high pressure torsion. *Acta Mater.* **2019**, *166*, 168–177. [CrossRef]
13. Gao, B.; Hu, R.; Pan, Z.; Chen, X.; Liu, Y.; Xiao, L.; Cao, Y.; Li, Y.; Lai, Q.; Zhou, H. Strengthening and ductilization of laminate dual-phase steels with high martensite content. *J. Mater. Sci. Technol.* **2021**, *65*, 29–37. [CrossRef]
14. Gao, B.; Chen, X.; Pan, Z.; Li, J.; Ma, Y.; Cao, Y.; Liu, M.; Lai, Q.; Xiao, L.; Zhou, H. A high-strength heterogeneous structural dual-phase steel. *J. Mater. Sci.* **2019**, *54*, 12898–12910. [CrossRef]
15. Li, J.; Cao, Y.; Gao, B.; Li, Y.; Zhu, Y. Superior strength and ductility of 316L stainless steel with heterogeneous lamella structure. *J. Mater. Sci.* **2018**, *53*, 10442–10456. [CrossRef]
16. Yang, Z.; Jiang, F.; Wang, Y.; Wang, Q.; Huang, M.; Wang, Y.; Chen, C.; Zhang, F. Making composite steel higher strength and higher ductility via introducing carbon diffusion strategy. *Mater. Res. Lett.* **2021**, *9*, 391–397. [CrossRef]
17. Ueji, R.; Tsuji, N.; Minamino, Y.; Koizumi, Y. Ultragrain refinement of plain low carbon steel by cold-rolling and annealing of martensite. *Acta Mater.* **2002**, *50*, 4177–4189. [CrossRef]

18. Yuan, Q.; Wang, Z.; Zhang, Y.; Ye, J.; Huang, Y.; Huang, A. Effect of Warm Rolling Temperature on the Microstructure and Texture of Microcarbon Dual-Phase (DP) Steel. *Metals* **2020**, *10*, 566. [CrossRef]
19. Xu, W.; Liu, X.C.; Li, X.Y.; Lu, K. Deformation induced grain boundary segregation in nanolaminated Al–Cu alloy. *Acta Mater.* **2020**, *182*, 207–214. [CrossRef]
20. Darling, K.A.; Srinivasan, S.; Koju, R.K.; Hornbuckle, B.C.; Smeltzer, J.; Mishin, Y.; Solanki, K.N. Stress-driven grain refinement in a microstructurally stable nanocrystalline binary alloy. *Scripta Mater.* **2021**, *191*, 185–190. [CrossRef]
21. Blum, W.; Dvořák, J.; Král, P.; Eisenlohr, P.; Sklenička, V. Strain Rate Contribution due to Dynamic Recovery of Ultrafine-Grained Cu–Zr as Evidenced by Load Reductions during Quasi-Stationary Deformation at 0.5 Tm. *Metals* **2019**, *9*, 1150. [CrossRef]
22. Xie, S.L.; Divinski, S.V.; Lei, Y.B.; Wang, Z.B. Accelerated grain boundary migration in nanolaminated interstitial-free steel during chromizing. *Mater. Res. Lett.* **2021**, *9*, 84–90. [CrossRef]
23. Lu, K. Stabilizing nanostructures in metals using grain and twin boundary architectures. *Nature Rev. Mater.* **2016**, *1*, 16019. [CrossRef]
24. Yan, C.K.; Feng, A.H.; Qu, S.J.; Cao, G.J.; Sun, J.L.; Shen, J.; Chen, D.L. Dynamic recrystallization of titanium: Effect of pre-activated twinning at cryogenic temperature. *Acta Mater.* **2018**, *154*, 311–324. [CrossRef]
25. Gao, B.; Lai, Q.; Cao, Y.; Hu, R.; Xiao, L.; Pan, Z.; Liang, N.; Li, Y.; Sha, G.; Liu, M.; et al. Ultrastrong low-carbon nanosteel produced by heterostructure and interstitial mediated warm rolling. *Sci. Adv.* **2020**, *6*, eaba8169. [CrossRef]
26. Araki, S.; Mashima, K.; Masumura, T.; Tsuchiyama, T.; Takaki, S.; Ohmura, T. Effect of grain boundary segregation of carbon on critical grain boundary strength of ferritic steel. *Scripta Mater.* **2019**, *169*, 38–41. [CrossRef]
27. Ahmadian, A.; Scheiber, D.; Zhou, X.; Gault, B.; Liebscher, C.H.; Romaner, L.; Dehm, G. Aluminum depletion induced by co-segregation of carbon and boron in a bcc-iron grain boundary. *Nat. Commun.* **2021**, *12*, 6008. [CrossRef]
28. Jiao, Z.B.; Luan, J.H.; Guo, W.; Poplawsky, J.D.; Liu, C.T. Atom-probe study of Cu and NiAl nanoscale precipitation and interfacial segregation in a nanoparticle-strengthened steel. *Mater. Res. Lett.* **2017**, *5*, 562–568. [CrossRef]
29. Lai, Q.; Brassart, L.; Bouaziz, O.; Gouné, M.; Verdier, M.; Parry, G.; Perlade, A.; Bréchet, Y.; Pardoen, T. Influence of martensite volume fraction and hardness on the plastic behavior of dual-phase steels: Experiments and micromechanical modeling. *Inter. J. Plast.* **2016**, *80*, 187–203. [CrossRef]
30. Xu, S.S.; Liu, Y.W.; Zhang, Y.; Luan, J.H.; Li, J.P.; Sun, L.X.; Jiao, Z.B.; Zhang, Z.W.; Liu, C.T. Precipitation kinetics and mechanical properties of nanostructured steels with Mo additions. *Mater. Res. Lett.* **2020**, *8*, 187–194. [CrossRef]
31. Du, C.; Hoefnagels, J.P.M.; Vaes, R.; Geers, M.G.D. Block and sub-block boundary strengthening in lath martensite. *Scr. Mater.* **2016**, *116*, 117–121. [CrossRef]
32. Li, S.; Zhu, G.; Kang, Y. Effect of substructure on mechanical properties and fracture behavior of lath martensite in 0.1C–1.1Si–1.7Mn steel. *J. Alloy. Compd.* **2016**, *675*, 104–115. [CrossRef]
33. Krauss, G. Martensite in steel: Strength and structure. *Mater. Sci. Eng. A* **1999**, *273–275*, 40–57. [CrossRef]
34. Ismail, K.; Perlade, A.; Jacques, P.J.; Pardoen, T. Outstanding cracking resistance of fibrous dual phase steels. *Acta Mater.* **2021**, *207*, 116700. [CrossRef]
35. Xu, Y.; Dan, W.; Ren, C.; Huang, T.; Zhang, W. Study of the Mechanical Behavior of Dual-Phase Steel Based on Crystal Plasticity Modeling Considering Strain Partitioning. *Metals* **2018**, *8*, 782. [CrossRef]
36. Zhu, Y.; Ameyama, K.; Anderson, P.M.; Beyerlein, I.J.; Gao, H.; Kim, H.S.; Lavernia, E.; Mathaudhu, S.; Mughrabi, H.; Ritchie, R.O.; et al. Heterostructured materials: Superior properties from hetero-zone interaction. *Mater. Res. Lett.* **2021**, *9*, 1–31. [CrossRef]
37. Jung, M.; Lee, S.J.; Lee, Y.K. Microstructural and Dilatational Changes during Tempering and Tempering Kinetics in Martensitic Medium-Carbon Steel. *Metall. Mater. Trans. A* **2009**, *40*, 551–559. [CrossRef]
38. Waterschoot, T.; Verbeken, K.; De Cooman, B.C. Tempering Kinetics of the Martensitic Phase in DP Steel. *ISIJ Inter.* **2006**, *46*, 138–146. [CrossRef]
39. Morsdorf, L.; Emelina, E.; Gault, B.; Herbig, M.; Tasan, C.C. Carbon redistribution in quenched and tempered lath martensite. *Acta Mater.* **2021**, *205*, 116521. [CrossRef]
40. Han, Q.; Kang, Y.; Hodgson, P.D.; Stanford, N. Quantitative measurement of strain partitioning and slip systems in a dual-phase steel. *Scr. Mater.* **2013**, *69*, 13–16. [CrossRef]
41. Diehl, M.; An, D.; Shanthraj, P.; Zaefferer, S.; Roters, F.; Raabe, D. Crystal plasticity study on stress and strain partitioning in a measured 3D dual phase steel microstructure. *Phys. Mesomech.* **2017**, *20*, 311–323. [CrossRef]
42. Djaziri, S.; Li, Y.; Nematollahi, G.A.; Grabowski, B.; Goto, S.; Kirchlechner, C.; Kostka, A.; Doyle, S.; Neugebauer, J.; Raabe, D.; et al. Deformation-Induced Martensite: A New Paradigm for Exceptional Steels. *Adv. Mater.* **2016**, *28*, 7753–7757. [CrossRef]
43. Li, Y.J.; Choi, P.; Borchers, C.; Westerkamp, S.; Goto, S.; Raabe, D.; Kirchheim, R. Atomic-scale mechanisms of deformation-induced cementite decomposition in pearlite. *Acta Mater.* **2011**, *59*, 3965–3977. [CrossRef]
44. Chen, S.Y.; Wang, L.; Li, W.D.; Tong, Y.; Tseng, K.K.; Tsai, C.W.; Yeh, J.W.; Ren, Y.; Guo, W.; Poplawsky, J.D.; et al. Peierls barrier characteristic and anomalous strain hardening provoked by dynamic-strain-aging strengthening in a body-centered-cubic high-entropy alloy. *Mater. Res. Lett.* **2019**, *7*, 475–481. [CrossRef]
45. Aboulfadl, H.; Deges, J.; Choi, P.; Raabe, D. Dynamic strain aging studied at the atomic scale. *Acta Mater.* **2015**, *86*, 34–42. [CrossRef]
46. Ye, C.; Suslov, S.; Kim, B.J.; Stach, E.A.; Cheng, G.J. Fatigue performance improvement in AISI 4140 steel by dynamic strain aging and dynamic precipitation during warm laser shock peening. *Acta Mater.* **2011**, *59*, 1014–1025. [CrossRef]

47. Bayramin, B.; Şimşir, C.; Efe, M. Dynamic strain aging in DP steels at forming relevant strain rates and temperatures. *Mater. Sci. Eng. A* **2017**, *704*, 164–172. [CrossRef]
48. Ekrami, A. High temperature mechanical properties of dual phase steels. *Mater. Lett.* **2005**, *59*, 2070–2074. [CrossRef]
49. Queiroz, R.R.U.; Cunha, F.G.G.; Gonzalez, B.M. Study of dynamic strain aging in dual phase steel. *Mater. Sci. Eng. A* **2012**, *543*, 84–87. [CrossRef]
50. Yan, N.; Li, Z.; Xu, Y.; Meyers, M.A. Shear localization in metallic materials at high strain rates. *Prog. Mater. Sci.* **2021**, *119*, 100755. [CrossRef]
51. Malheiros, L.R.C.; Rodriguez, E.A.P.; Arlazarov, A. Mechanical behavior of tempered martensite: Characterization and modeling. *Mater. Sci. Eng. A* **2017**, *706*, 38–47. [CrossRef]
52. Zhao, P.; Wang, Y.; Niezgoda, S.R. Microstructural and micromechanical evolution during dynamic recrystallization. *Inter. J. Plast.* **2018**, *100*, 52–68. [CrossRef]
53. Souza, R.C.; Silva, E.S.; Jorge, A.M.; Cabrera, J.M.; Balancin, O. Dynamic recovery and dynamic recrystallization competition on a Nb- and N-bearing austenitic stainless steel biomaterial: Influence of strain rate and temperature. *Mater. Sci. Eng. A* **2013**, *582*, 96–107. [CrossRef]
54. Wang, W.; Yuan, F.; Wu, X. Smaller critical size and enhanced strength by nano-laminated structure in nickel. *Comp. Mater. Sci.* **2015**, *110*, 83–90. [CrossRef]
55. Zeng, L.F.; Gao, R.; Fang, Q.F.; Wang, X.P.; Xie, Z.M.; Miao, S.; Hao, T.; Zhang, T. High strength and thermal stability of bulk Cu/Ta nanolamellar multilayers fabricated by cross accumulative roll bonding. *Acta Mater.* **2016**, *110*, 341–351. [CrossRef]
56. Zhu, Y.; Li, Z.; Huang, M.; Liu, Y. Strengthening mechanisms of the nanolayered polycrystalline metallic multilayers assisted by twins. *Inter. J. Plast.* **2015**, *72*, 168–184. [CrossRef]